Ceramics-Silikáty 67 (1), 29-36 (2023)
www.ceramics-silikaty.cz
doi: 10.13168/cs.2022.0057

Ni-BZCYYb HYDROGEN SEPARATION MEMBRANE FOR THE INTEGRATION OF HYDROGEN PRODUCTION AND HYDROGEN SEPARATION BY ETHANOL REFORMING

ZHIJIN DAI*, #FENGHUA JIANG*

**School of Materials Science and Engineering, University of Jinan, Jinan 250022, P.R. China*

#E-mail: mse_jiangfh@ujn.edu.cn

Submitted November 25, 2022; accepted December 23, 2022

Keywords: hydrogen separation membrane, fibre catalyst, ethanol reforming, integration, surface exchange

The integration of hydrogen production and hydrogen separation is achieved in this study by combining the membrane technology for hydrogen separation with the biomass ethanol reforming hydrogen production. At various temperatures, the impact of the surface exchange on the hydrogen permeability was investigated, and a Pd-GDC catalyst helped to overcome the surface exchange's bottlenecks. When the Pd-GDC catalyst was added, the hydrogen permeation fluxes of the Ni-BZCYYb hydrogen separation membrane made by a mesh-assisted phase-inversion process can achieve 0.730 ml cm^{-2}·min^{-1} at 850 °C and can be stably maintained for 100 hours. The ethanol conversion rate can be increased to 70 % with the addition of an Ru-GDC fibre catalyst into the channel's feeding side and building a micro reformer for efficient ethanol water reforming. Additionally, the hydrogen permeation fluxes can increase to 0.717 ml cm^{-2}·min^{-1} and can be stably maintained for 100 hours. This study shows how to produce and separate pure hydrogen energy from renewable ethanol in an effective manner.

INTRODUCTION

Hydrogen, the highest combustion energy density and environmental protection energy source, has long garnered a lot of attention [1]. At the moment, methane reforming reactions are frequently used in industry to produce hydrogen [2]. The technique is unsustainable due to the substantial emissions of carbon compounds and the dependence on non-renewable fossil fuels.

With a high combustion energy density and a non-toxic liquid state at room temperature, ethanol is a renewable energy source that can be produced from biomass, which is easy to store and transport [3]. The benefits of ethanol water reformation to hydrogen production have drawn a lot of study attention since it has been demonstrated that ethanol can restructure hydrogen on fuel cells [4-6]. The highest hydrogen production in ethanol water reformation can be seen from the reactions that follow:

$$C_2H_5OH + 3H_2O = 2CO_2 + 6H_2 \qquad (1)$$

However, ethanol water reformation simultaneously experiences complex side reactions at high temperatures [7], including:

$$C_2H_5OH = CH_4 + H_2 + CO \qquad (2)$$

$$C_2H_5OH = C_2H_4 + H_2O \qquad (3)$$

$$C_2H_5OH = C_2H_4O + H_2O \qquad (4)$$

$$CH_4 + H_2O = 2CO_2 + 4H_2 \qquad (5)$$

$$CH_4 = C + H_2 \qquad (6)$$

$$2CO = CO_2 + C \qquad (7)$$

$$CO + H_2O = CO_2 + H_2 \qquad (8)$$

The by-products from these reactions, such CO_2, CH_4, C_2H_4O, C_2H_4, and C, result in carbon coking, which deactivates the catalyst [8, 9].

The industry uses the pressure swing adsorption method to separate hydrogen in order to obtain pure hydrogen energy [10]. This method continuously purifies hydrogen in a quick cycle, but it requires a great deal of energy during the low-temperatures distillation step and additional high pressure, which has high safety requirements for the entire production process. Due to high hydrogen selectivity and low energy requirement, hydrogen can be efficiently purified on a large-scale using hydrogen separation membranes [11, 12]. The pricey Pd metal separation membrane has high hydrogen selectivity and only one billionth of an impurity concentration in the separated product, but it is simple for the Pd lattice to go through an irreversible phase transition at high temperatures, leading to membrane structural failure [12]. Due to its high selectivity, low energy consumption, low cost, and strong mechanical qualities, ceramic separation membranes based on proton conductors have gar-nered scientific interest [13, 14]. A metal conductor and a high-temperature proton conductor make up the ceramic separation membrane [15]. On the one hand, at high temperatures, proton conductors offer improved H^+ proton conduction channels for dense ceramic membrane. According to reports, $BaZr_{0.1}Ce_{0.7}Y_{0.1}Yb_{0.1}O_3$ (BZCYYb) demonstrates excellent proton conductivity as well as good chemical and thermal stability in an environment comprising H_2O and CO_2 [16]. On the other hand, metal conductors offer e^- channels. Ni has strong conductivity and catalytic activity, which is employed frequently in fuel cells [17, 18]. Further decreasing the complexity of the systems for producing and separating hydrogen at high temperatures is the use of Ni as a catalyst for the reforming of fossil fuels [19].

Hydrogen adsorption, proton electron conduction, and hydrogen dissociation are the three key steps in the process of separating hydrogen using a ceramic membrane [20]. The hydrogen penetration fluxes is inversely related to the thickness of the penetration layer until it is below 80 µm [21], according to reports, and when the thickness of the penetration layer is decreased, a shorter transmission channel for H^+ and e^- is created. The exchange kinetics play a major role in controlling the hydrogen penetration below this thickness [22]. Dong et al. [21] prepared a ceramic vertical channel structure using the mesh-assisted phase-inversion process. The inverted U-shaped structure of the hydrogen adsorption side of the ceramic separation membrane provided more contact sites between the gas and the dense penetration layer, and the vertical channel promoted the permeability of the reactive gas directly reaching the hydrogen adsorption side of the membrane. The results demonstrated that vertical channel is a promising configuration for significantly enhancing the surface adsorption [23, 24]. In this study, we have created a new ceramic hydrogen separation membrane that efficiently lowers the surface adsorption limitations and integrates the production of hydrogen from ethanol reformation and hydrogen separation.

EXPERIMENTAL

Hydrogen separation membrane fabrication

By using a conventional solid-state reaction (SSR), a BZCYYb powder was made. Ball milling stoichiometric proportions of $BaCO_3$, ZrO_2, CeO_2, Y_2O_3, and Yb_2O_3 in ethanol for 24 hours was followed by drying, grinding, then the mixture was calcined for 10 hours at 1150 °C, this process was repeated up till a pure perovskite phase was formed. According to the volume ratio of 6:4, the BZCYYb/NiO powder was evenly combined. The mesh-assisted phase-inversion process [25] described in our prior study was used to create the BZCYYb-NiO support body. The support body was calcined at 400 °C for one hour to burn the polymer, and then at 1050 °C for two hours to obtain the necessary mechanical strength. A permeable slurry was created by combining 3 g of BZCYYb and NiO (volume 6:4) with 30 ml of ethanol in a ball mill for 24 hours. This slurry was then impregnated into the smooth surface of the support body. By calcining at 1450 °C for 300 min in a 5 % H_2/Ar environment, the BZCYYb-NiO hydrogen separation membrane with an inverted U-shaped inner surface and vertical channel was created. Different thicknesses of the dense hydrogen permeation layer between 10 and 30 µm can be regulated.

Catalyst fabrication

A Pd- Gadolinium doped ceria (Pd-GDC) catalyst was created to enhance the surface exchange between the hydrogen and the hydrogen permeation layer [26]. With a syringe, the Pd-GDC catalyst solution was added in a dropwise fashion at a ratio of 5 mg·cm^{-2} to the feeding side of the hydrogen separation membrane. After drying, calcining for two hours at 800 °C, a 5 wt. % Ru/GDC [27] fibre catalyst was made by electrospinning and then calcining at 800 °C for two hours in order to increase the efficiency of the ethanol reforming. By ultrasonically stirring, 10 ml of ethanol and a 50 µm fibre catalyst were mixed. Following that, the resultant solution was applied to the feeding side of the separation membrane and allowed to dry. The procedure was repeated until the additional concentration reached 4 mg·cm^{-2}. Scanning electron microscope (SEM, Phenom, ProX, the Netherlands) was used to examine the interior structure of the hydrogen separation membrane. Figure 1 shows the workings of the hydrogen separation membrane and the ethanol reformation. In the vertical channel, ethanol was reformed to produce hydrogen, and pure hydrogen energy was separated by the dense hydrogen penetration layer.

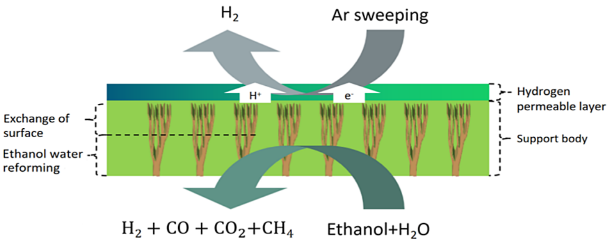

Figure 1. Schematic diagram of the ethanol water reformation and hydrogen separation.

Hydrogen separation measurements

For the measurements of the ethanol water reforming and hydrogen separation, a homemade instrument (shown in Figure 2) was used. The porous surface was heat-bonded to the top of the feeding side using ceramic adhesive. The hydrogen separation membrane has an effective surface area of 0.6/cm^2. Humidified 3 vol. % H_2O, Ar, N_2, and various concentrations of an H_2 mixture are used in the feeding side for a 50 ml·min^{-1} total flow rate to test the hydrogen permeability. 50 ml·min^{-1} Ar was used as the sweeping gas and supplied into the gas chromatograph (GC) (Shimadzu GC-2014) to assess the hydrogen permeation fluxes. The following formula can be used to determine the airtightness – η:

$$\eta = 1 - Cf(H_2)/Cf(N_2) \times Cp(N_2)/Cp(H_2),$$

where $Cp(H_2)$, $Cp(N_2)$, $Cf(H_2)$, and $Cf(N_2)$ stand for the concentrations of H_2 and N_2 on the feeding side and sweeping side, respectively. The airtightness stayed above 97 % during the test. The following formula can be used to determine hydrogen permeation fluxes:

$$JH_2 = F \times [1 - Cf(H_2)/Cf(N_2) \times Cp(N_2)/Cp(H_2)]/A,$$

where F and A stand for the effective area of the hydrogen membrane and the overall gas flow rate on the feeding side, respectively.

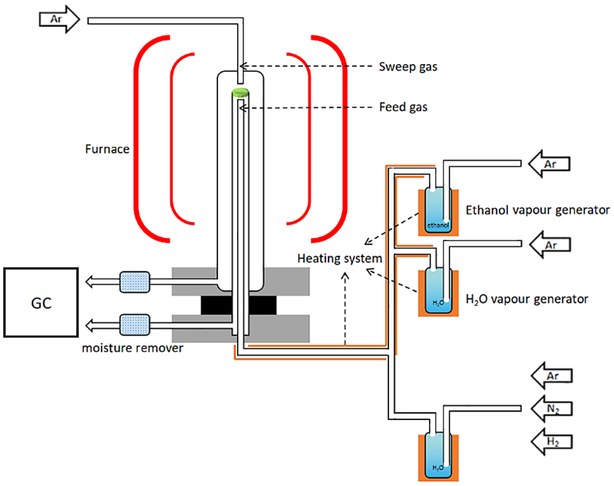

Figure 2. Test device of the ethanol reforming hydrogen production and separation.

In the ethanol water reforming and hydrogen separation test, the sweeping side was kept at 50 ml·min^{-1} of Ar sweeping and fed into the GC, while the feed gas consisted of 40 ml·min^{-1} Ar loaded with H_2O and 10 ml·min^{-1} Ar loaded with ethanol. The ideal concentrations of ethanol and H_2O were ultimately confirmed to be 7.5 % and 10 %, respectively, by altering the relationship between the temperature and saturated vapour pressure. The GC was then used to test the selectivity of the hydrogen and the conversion rate of the ethanol using the reforming gas on the feeding side.

RESULTS AND DISCUSSION

The overall morphology of the hydrogen separation membrane is depicted in Figure 3. The hydrogen separation membrane's vertical feeding side channel makes it easier to transfer gas and load the fibre catalyst. The vertical channel breaks into several parallel narrow vertical channels, then splits once more to reach the inner surface of the permeation layer. When approaching the permeation layer, Figure 3b shows a dense inverted U-shaped structure that effectively increases the contact area for the feed gas and hydrogen permeation layer to boost the capacity of the hydrogen adsorption [25]. The permeation layer is dense and just 10 µm thick, which not only successfully reduces the transmission resistance of H^+ and e^-, but also guarantees the permeation layer's airtightness. Additionally, the Ru-GDC fibre catalyst is successfully added into the vertical channel of the support body (Figure 3e) to encourage the reforming of ethanol into hydrogen.

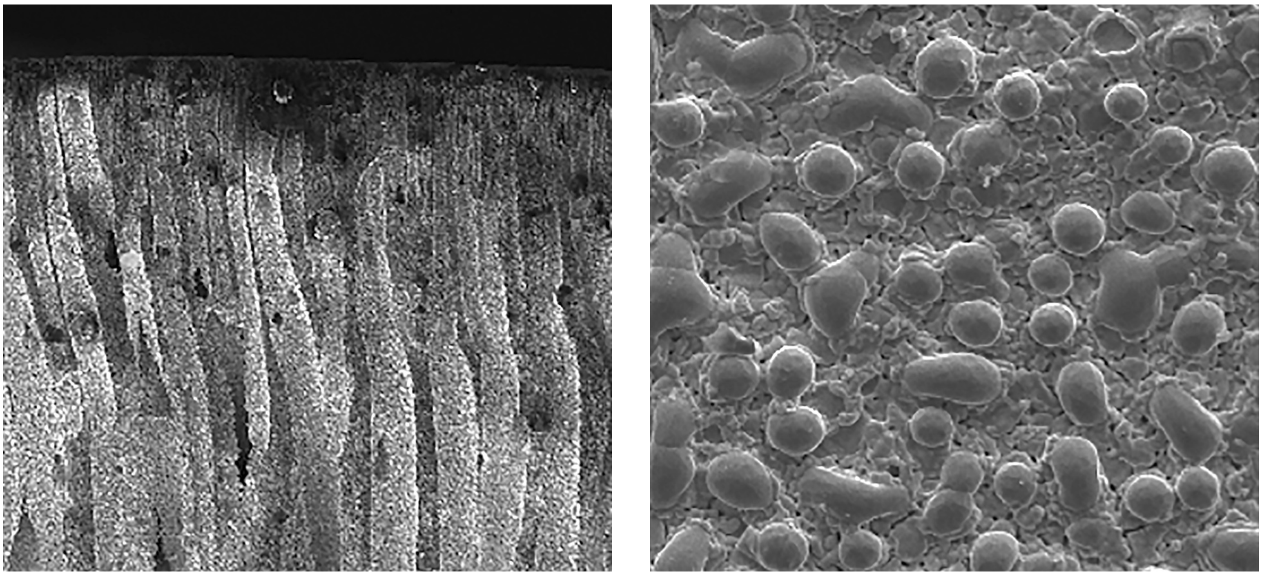
a)

b)

Figure 3. Microstructure of: a) SEM image of the cross-sectional view of the dense permeation layer on the porous Ni-BZCYYb supports; b) High magnification SEM image of the dense surface of the hydrogen permeation layer. *(Continue on next page)*

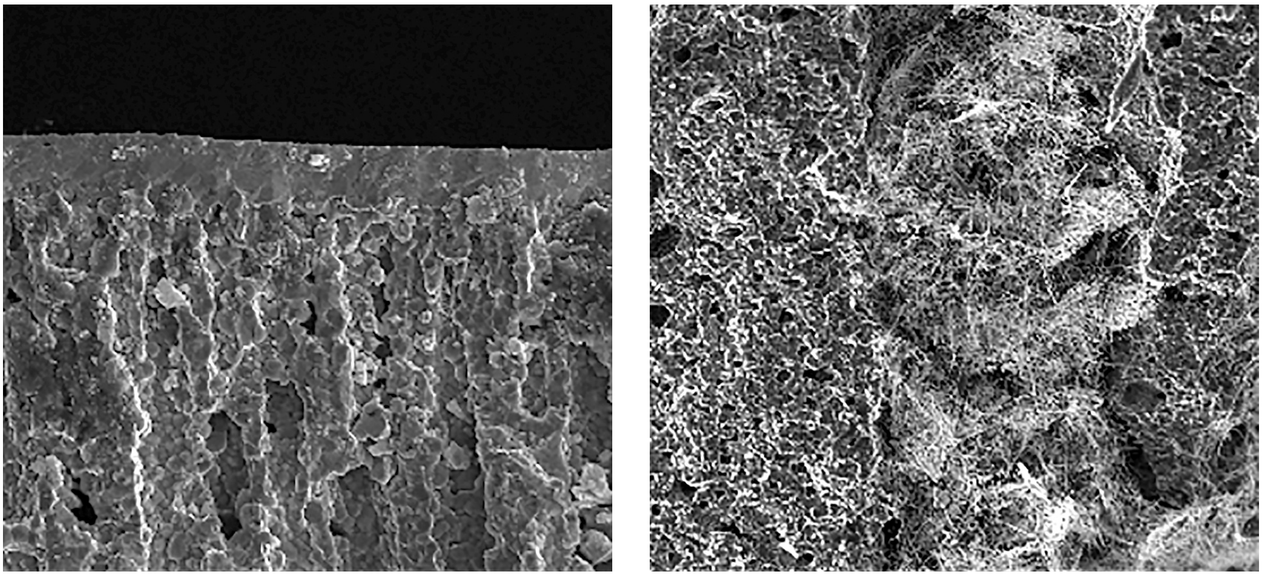
c)
d)

Figure 3. Microstructure of: c) High magnification SEM image of the connection between the dense permeation layer and the vertical channels; d) High magnification SEM image of the Ru-GDC fibre catalyst filling in the vertical channels.

Figure 4 shows the hydrogen permeation fluxes of the 15 µm thick dense layer of the Ni-BZCYYb hydrogen separation membrane, as it was constructed at various feed gas hydrogen partial pressures and operation temperatures. When pure hydrogen was added to the feeding side, the hydrogen permeation fluxes in-creased from to 0.850 ml·cm^{-2}·min^{-1} as the temperature was increased from 650 °C to 850 °C. When 20 % hydrogen was added to the feeding side, the hydrogen permeation fluxes increased from 0.214 to 0.545 ml·cm^{-2}·min^{-1} as the temperature was increased from 650 °C to 850 °C. The hydrogen permeation fluxes are maintained at a high level in the proton-conductor-based ceramic hydrogen separation membranes [21, 22, 28]. The discovered efficient hydrogen permeation fluxes may be due to the ionic conductivity of the BZCCYb and Ni [16, 17, 29]. The newly designed hydrogen separation membrane has an inverted U-shaped interface that offers more hydrogen reaction sites than conventional asymmetric hydrogen separation membranes, and the vertical channel can maintain a smooth feed gas transfer.

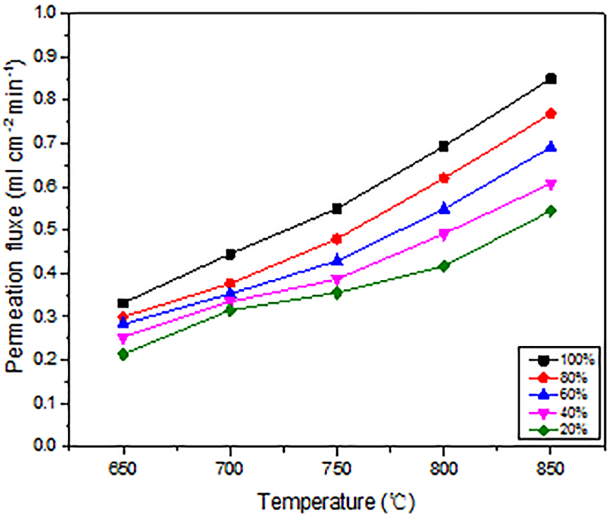

Figure 4. Hydrogen permeation fluxes of the 15 µm thick dense layer of the Ni-BZCYYb membrane under different feed gas hydrogen partial pressures and various temperatures.

However, the hydrogen permeation fluxes do not increase when the thickness of permeation layer is less than 15 µm, thus we investigated the correlation between the hydrogen permeation fluxes and the thickness of the hydrogen permeation layer. Figure 5a shows that the thickness reduced from 30 µm to 15 µm, and the hydrogen permeation fluxes increased from 0.401 to 0.545 ml·cm^{-2}·min^{-1} and from 0.129 to 0.214 ml·cm^{-2}·min^{-1} at 850 °C and 650 °C, respectively. However, at any temperatures, the hydrogen permeation fluxes did not increase as the thickness was further decreased to 10 µm. This circumstance also occurred when the permeation layer was thinner than 80 µm, according to Song's research on the inverse relationship between the permeation fluxes and the thickness [21]. This study shows that the new separation membrane has a larger surface exchange capacity as it occurs in our hydrogen separation membrane when the permeation layer thickness reaches 20 µm. At 650 °C, there is a linear relationship between the hydrogen permeability of the 30 µm and 15 µm thicknesses, but this relationship weakens with the temperature increase. We conclude from this that when the permeation layer reduced to a certain thickness, the temperature increases the surface exchange limiting factor.

Figure 5b shows the influence of the temperature and thickness on the hydrogen permeation fluxes both before and after the addition of the Pd-GDC catalyst. The hydrogen permeation fluxes increased from 0.217 to 0.370 ml·cm^{-2}·min^{-1} and from 0.549 to 0.730 ml·cm^{-2}·min^{-1} at 650 °C and 850 °C, respectively, when the thickness of the hydrogen permeation layer was 10 μm after the Pd-GDC catalyst was added. The adsorption capacity of hydrogen is significantly enhanced by the addition of the PD-GDC catalyst [26], increasing the hydrogen permeation fluxes. Consequently, it can be concluded that the hydrogen separation membrane of the vertical channel is a hydrogen separation membrane that can be effectively adjusted utilising the catalyst. The hydrogen permeation fluxes increased from 0.218 to 0.370 ml·cm^{-2}·min^{-1} and from 0.598 to 0.730 ml·cm^{-2}·min^{-1} at 650 °C and 850 °C, respectively, when the thickness of the hydrogen separation membrane with the catalyst was decreased from 15 μm to 10 μm. The adsorption capacity of hydrogen is significantly enhanced by the addition of PD-GDC, increasing the hydrogen permeation fluxes [26]. At higher temperatures, the effect of the PD-GDC addition is more obvious in reducing the limiting factors brought on by the surface exchange. Consequently, it can be concluded that the hydrogen separation membrane of the vertical channel is a hydrogen separation membrane that can be effectively adjusted utilising the catalyst. The hydrogen permeation fluxes follow a linear relationship with the thickness at 650 °C, but over 650 °C, as the thickness drops, the surface limiting factors become more significant. This leads us to conclude that the surface exchange limits the hydrogen permeation fluxes to a greater extent at higher temperatures. The transport capacity of H$^+$ and e$^-$ increases with the temperature, but the amount of H$_2$ consumed for surface adsorption does not correspondingly increase. Due to the inability to supply more H$^+$ and e$^-$ for transportation, the hydrogen separation cannot accordingly increase as a result [21, 30]. Finally, with the addition of the Pd-GDC catalyst, which increased the adsorption capacity, the hydrogen permeation fluxes of the 10 μm hydrogen permeation layer can reach 0.730 ml·cm^{-2}·min^{-1} and be stable for 100 hours. It shows that throughout the testing, the Ni-BZCYYb hydrogen separation membrane with vertical channel does not undergo any phase transition or suffer any major structural degradation. The potential of the vertical channel for hydrogen separation is demonstrated by its high permeation efficiency and steady permeation output.

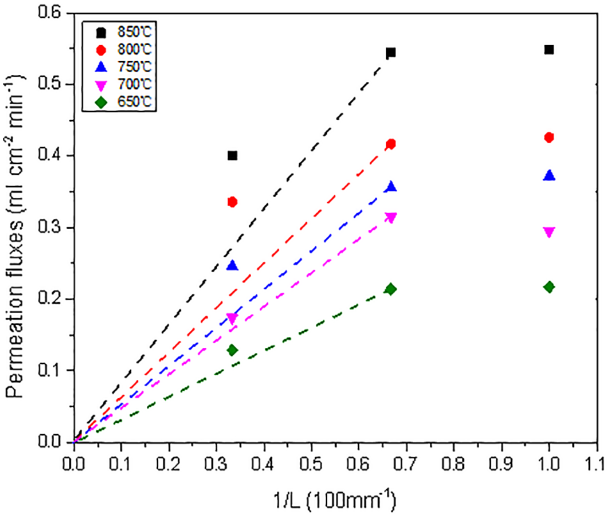

a)

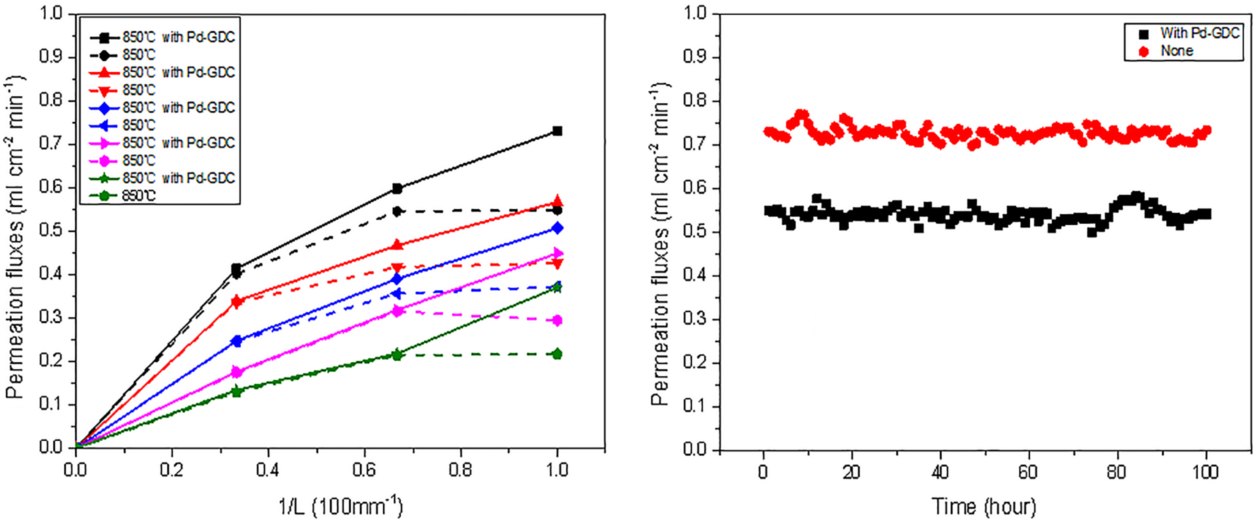

b) c)

Figure 5. a) Hydrogen permeation fluxes of a 10 - 30 μm thick dense layer of the Ni-BZCYYb membrane at 650 - 850 °C without a catalyst; b) Changes in the amount of hydrogen permeation fluxes of the 10 - 30 μm thick dense layer of the Ni-BZCYYb membrane at 650 - 850 °C with the addition of the Pd-GDC catalyst; c) Hydrogen permeation fluxes within 100 hours when 50 ml·cm^{-2}·min^{-1} H$_2$/AR(20 %H$_2$) was fed into the separation membrane with the 10 μm thick dense layer.

Figure 6 shows the ethanol reforming gas composition in the hydrogen separation membrane of a 10 μm permeation layer without the Ru-GDC fibre catalyst. The hydrogen production increased from 4.06 to 6.62 ml·cm^{-2}·min^{-1} when the temperature was increased from 750 °C to 850 °C. Ni is an effective catalyst [26] by nature, and the vertical pores offer a favourable environment for Ni to reform catalytically [31]. Figure 6b shows the hydrogen production value increased from 6.70 ml·cm^{-2}·min^{-1} to 9.30 ml·cm^{-2}·min^{-1} when the temperature was increased from 750 °C to 850 °C with the addition of the Ru-GDC fibre catalyst. The ethanol reforming reaction gradually shifted from Ni to the Ru-GDC fibre catalyst after the catalyst addition. The hydrogen production yield is effectively increased by the addition of the Ru-GDC fibre catalyst.

Figure 7a shows that with the addition of the RU-GDC fibre catalyst, the conversion rate of ethanol increased from 40.53 % to 60.15 % when the temperature was increased from 750 °C to 850 °C, while the selectivity

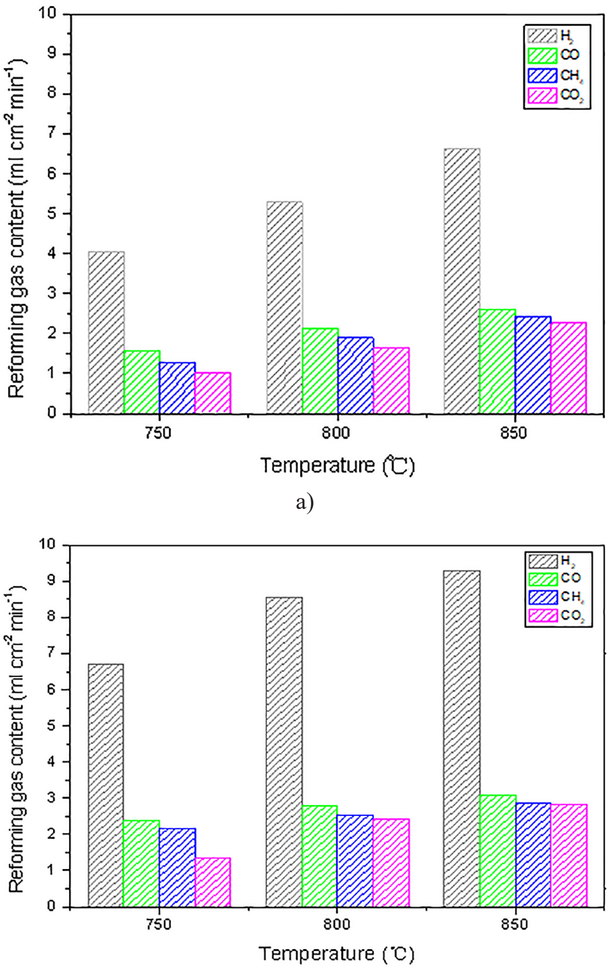

a)

b)

Figure 6. The composition of the ethanol reforming gas at 750 °C - 850 °C: a) without the Ru-GDC fibre catalyst; b) with the Ru-GDC fibre catalyst when 7.5 % ethanol was fed into the separation membrane with a 10 μm thick dense layer.

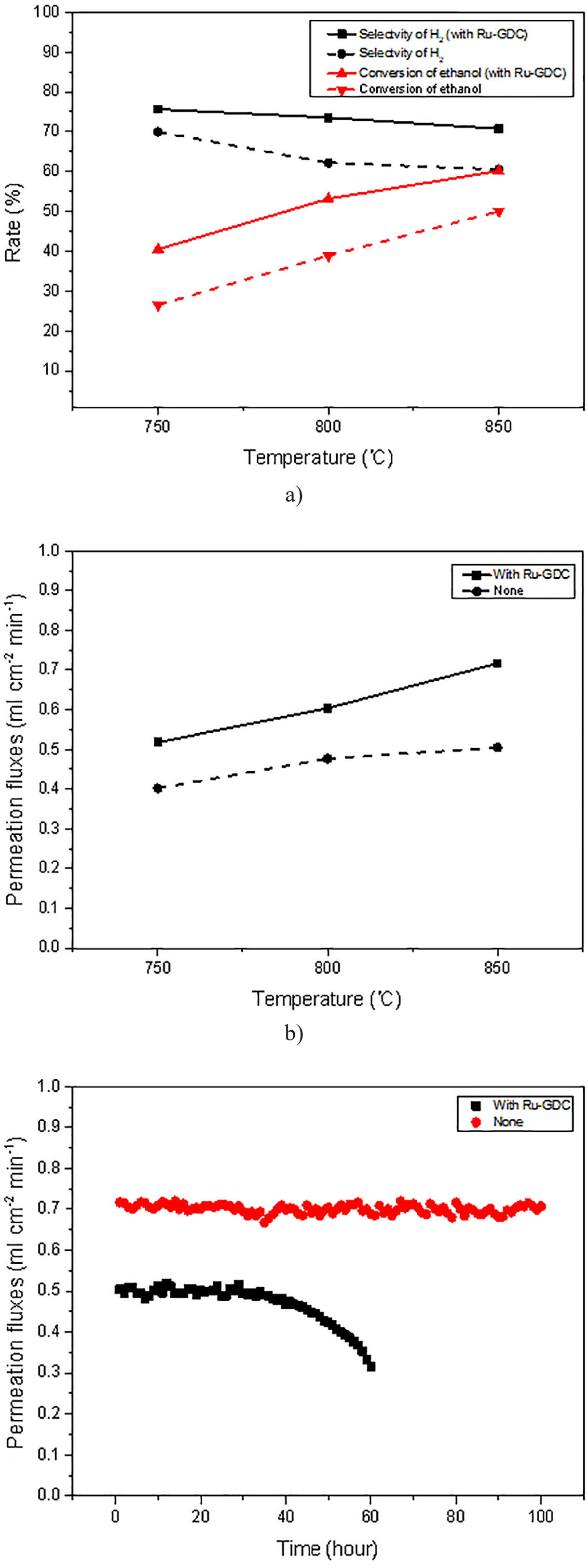

a)

b)

c)

Figure 7. a) Conversion rate of the ethanol and selectivity of the hydrogen at 750 °C to 850 °C before and with the addition of the Ru-GDC fibre catalyst; b) Hydrogen permeation fluxes that separate during the reforming of ethanol before and after the addition of the Ru-GDC fibre catalyst.

of hydrogen remained above 70 %. The efficiency of the ethanol hydrogen production is significantly increased by the addition of the Ru-GDC fibre catalyst. When the temperature was increased from 750 °C to 850 °C, as shown in Figure 7b, without the addition of the RU-GDC fibre catalyst, the hydrogen permeation fluxes increased from 0.404 ml·cm^{-2}·min^{-1} to 0.505 ml·cm^{-2}·min^{-1}, while the hydrogen permeation fluxes increased from 0.518 ml·cm^{-2}·min^{-1} to 0.717 ml·cm^{-2}·min^{-1} after the addition of the Ru-GDC catalyst. The concentration of hydrogen in the reforming gas increases with the addition of the Ru-GDC fibre catalyst, increasing the hydrogen permeation fluxes. This proves that using this hydrogen separation membrane, it is feasible to use ethanol reforming to make hydrogen and separate hydrogen. Figure 7c shows that the production of hydrogen and the separation of ethanol water reforming can both remain stable for 100 hours with the addition of the Ru-GDC fibre catalyst, while without the addition of the fibre catalyst, the by-product of ethanol water reforming causes serious carbon coking, leading to the failure of the ethanol reforming and the failure to separate hydrogen [32]. The addition of the Ru-GDC fibre catalyst effectively weakens the carbon coking. This demonstrates how successfully ethanol reforming to produce hydrogen and separate hydrogen after adding fibre catalyst can be achieved using a hydrogen separation membrane with a vertical channel.

CONCLUSION

This study has created a novel hydrogen separation membrane in order to integrate hydrogen production and separation by ethanol water reforming. The redesigned structure and the addition of a Pd-GDC catalyst increased the hydrogen separation, and it was discovered that the surface exchange limiting factors increased with the temperature. The hydrogen permeation fluxes at various temperatures can be efficiently increased by adding a Pd-GDC catalyst. The hydrogen production, ethanol conversion effectiveness, and hydrogen selectivity are all enhanced by the addition of an RU-GDC fibre catalyst in the ethanol reforming process. The hydrogen separation membrane achieves ethanol water reforming and hydrogen separation while maintaining stability. The integration of the hydrogen production from the ethanol reformation and separation is, therefore, made possible by the hydrogen separation membrane with a vertical channel, showing its potential for use in the advancement of renewable energy.

REFERENCES

1. Staffel I.l, Scamman D., Velazquez Abad A., Balcombe P., Dodds P.E., Ekins P., Shah N., Ward K.R. (2019): The role of hydrogen and fuel cells in the global energy system. *Energy & Environmental Science, 12*, 463-491. doi: 10.1039/C8EE01157E
2. Wismann S.T., Engbæk J.S., Vendelbo S.B., Bendixen F.B., Eriksen W.L., Aasberg-Petersen K., Frandsen C., Chorkendorff I., Mortensen P.M. (2019): Electrified methane reforming: A compact approach to greener industrial hydrogen production. *Science, 364,* 756-759. doi: 10.1126/science.aaw8775
3. Greluk M., Rotko M., Turczyniak-Surdacka S. (2020): Enhanced catalytic performance of La$_2$O$_3$ promoted Co/CeO$_2$ and Ni/CeO$_2$ catalysts for effective hydrogen production by ethanol steam reforming. *Renewable Energy, 155,* 378-395. doi: 10.1016/j.renene.2020.03.117
4. Fierro V., Klouz V., Akdim O., Mirodatos C. (2002): Oxidative reforming of biomass derived ethanol for hydrogen production in fuel cell applications. *Catalysis Today, 75*, 141-144. doi: 10.1016/S0920-5861(02)00056-1
5. Deluga G.A., Salge J.R., Schmidt L.D., Verykios X.E. (2004): Renewable Hydrogen from Ethanol by Autothermal Reforming. *Science, 303*, 993-997. doi: 10.1126/science.1093045
6. Wang W., Wang Y. (2009): Dry reforming of ethanol for hydrogen production: Thermodynamic investigation. *International Journal of Hydrogen Energy, 34*, 5382-5389. doi: 10.1016/j.ijhydene.2009.04.054
7. Li N., Pu J., Chi B., Li J. (2019): Ethanol steam reforming with a Ni–BaZr$_{0.1}$Ce$_{0.7}$ Y$_{0.1}$Yb$_{0.1}$O$_{3-\delta}$ catalyst. *Materials Today Energy, 12*, 371-378. doi: 10.1016/j.mtener.2019.04.002
8. Farrell B., Linic S. (2016): Direct electrochemical oxidation of ethanol on SOFCs: Improved carbon tolerance of Ni anode by alloying. *Applied Catalysis B: Environmental, 183*, 386-393. doi: 10.1016/j.apcatb.2015.11.002
9. Wang W., Su C., Ran R., Zhao, B. Shao Z., Tade M. O., Liu S. (2014): Nickel-Based Anode with Water Storage Capability to Mitigate Carbon Deposition for Direct Ethanol Solid Oxide Fuel Cells. *ChemSusChem, 7*, 1719-1728. doi. 10.1002/cssc.201301341
10. Gallagher J. (2017): Hydrogen storage: Pressure swing. *Nature Energy, 2*. doi: 10.1038/nenergy.2017.122
11. Drioli E., Fontananova E. (2004): Membrane Technology and Sustainable Growth. *Chemical Engineering Research and Design, 82*, 1557-1562. doi: 10.1205/cerd.82.12.1557.58031
12. Shu J., Grandjean B.P.A., Neste A.V., Kaliaguine S. (1991): Catalytic palladium-based membrane reactors: A review. *The Canadian Journal of Chemical Engineering, 69*, 1036-1060. doi: 10.1002/cjce.5450690503
13. Phair J.W., Badwal S.P.S. (2006): Materials for separation membranes in hydrogen and oxygen production and future power generation. *Science and Technology of Advanced Materials, 7*, 792-805. doi: 10.1016/j.stam.2006.11.005
14. Hashim S.S., Somalu M.R., Loh K.S., Liu S., Zhou W., Sunarso J. (2018): Perovskite-based proton conducting membranes for hydrogen separation: A review. *International Journal of Hydrogen Energy, 43*, 15281-15305. doi: 10.1016/j.ijhydene.2018.06.045
15. Ernst B., Haag S., Burgard M. (2007): Permselectivity of a nickel/ceramic composite membrane at elevated temperatures: A new prospect in hydrogen separation? *Journal of Membrane Science, 288*, 208-217. doi: 10.1016/j.memsci.2006.11.017
16. Choi M., Paik J., Kim D., Woo D., Lee J., Kim S.J., Lee J., Lee W. (2021): Exceptionally high performance of protonic

ceramic fuel cells with stoichiometric electrolytes. *Energy & Environmental Science, 14,* 6476-6483. doi: 10.1039/D1EE01497H

17. Liu M., van der Kleij A., Verkooijen A.H.M., Aravind P.V. (2013): An experimental study of the interaction between tar and SOFCs with Ni/GDC anodes. *Applied Energy, 108*, 149-157. doi: 10.1016/j.apenergy.2013.03.020
18. Shri Prakash B., Senthil Kumar S., Aruna S.T. (2014): Properties and development of Ni/YSZ as an anode material in solid oxide fuel cell: A review. R*enewable and Sustainable Energy Reviews, 36*, 149-179. doi: 10.1016/j.rser.2014.04.043
19. Bepari S., Sarkar J.J., Pradhan N.C. (2022): Kinetics of ethanol steam reforming over Ni/Olivine catalyst. *International Journal of Hydrogen Energy, 47*, 30843-30860. doi: 10.1016/j.ijhydene.2022.02.032
20. Pal N., Agarwal M. (2021): Advances in materials process and separation mechanism of the membrane towards hydrogen separation. *International Journal of Hydrogen Energy, 46*, 27062-27087. doi: 10.1016/j.ijhydene.2021.05.175
21. Song S.J., Moon J.H., Lee T.H., Dorris S.E., Balachandran U. (2008): Thickness dependence of hydrogen permeability for Ni–BaCe$_{0.8}$Y$_{0.2}$O$_{3-\delta}$. *Solid State Ionics, 179,* 1854-1857. doi: 10.1016/j.ssi.2008.05.012
22. Zhu Z., unW. S, Yan L., Liu W., Liu W. (2011): Synthesis and hydrogen permeation of Ni–Ba(Zr$_{0.1}$Ce$_{0.7}$Y$_{0.2}$)O$_{3-\delta}$ metal – ceramic asymmetric membranes. *International Journal of Hydrogen Energy, 36*, 6337-6342. doi: 10.1016/j.ijhydene.2011.02.029
23. Wang R., Wang T., Ma Y., Wei T., Ye Z., Chen B., Dong D. (2022): Control of carbon deposition over methane-fueled SOFCs through tuning the O/C ratio at the anode/electrolyte interface. *Journal of Power Sources, 544*. doi: 10.1016/j.jpowsour.2022.231854
24. Ji G., Wang G., Hooman K., Bhatia S., Diniz da Costa J.C. (2012): Computational fluid dynamics applied to high temperature hydrogen separation membranes. *Frontiers of Chemical Science and Engineering, 6*, 3-12. doi: 10.1007/s11705-011-1161-5
25. Wang T., Tian Y., Li T., Yu L., Ye Z., Wei T., Wang Z., Yao J., Buckley C.E., Dong D. (2019): Essential microstructure of cathode functional layers of solid oxide electrolysis cells for CO$_2$ electrolysis. J*ournal of CO$_2$ Utilization, 32*, 214-218. doi: 10.1016/j.jcou.2019.04.021
26. Jia L., Hu T., Liang F., Liu M., Zhang Y., Jiang H. (2022): Enhanced CO$_2$-tolerance and hydrogen separation performance of Ba-based ceramic membrane modified by Ce$_{0.9}$Gd$_{0.1}$O$_{2-\delta}$ surface layer. *Separation and Purification Technology, 303*, 122246. doi: 10.1016/j.seppur.2022.122246
27. Ma Y., Ma Y., Zhao Z., Hu X., Ye Z., Yao J., Buckley C.E., Dong D. (2019): Comparison of fibrous catalysts and monolithic catalysts for catalytic methane partial oxidation. *Renewable Energy, 138,* 1010-1017. doi: 10.1016/j.renene.2019.02.027
28. Zuo C., Lee T.H., Dorris S.E., Balachandran U., Liu M. (2006): Composite Ni–Ba(Zr$_{0.1}$Ce$_{0.7}$Y$_{0.2}$)O$_3$ membrane for hydrogen separation. *Journal of Power Sources, 159*, 1291-1295. doi: 10.1016/j.jpowsour.2005.12.042
29. Zhu Z., Hou J., He W., Liu W. (2016): High-performance Ba(Zr$_{0.1}$Ce$_{0.7}$Y$_{0.2}$)O$_{3-\delta}$ asymmetrical ceramic membrane with external short circuit for hydrogen separation. *Journal of Alloys and Compounds,* 660, 231-234. doi: 10.1016/j.jallcom.2015.11.065
30. Zhu Z., Meng X., Liu W., Wei Z. (2019): Study on hydrogen permeation of Ni-BaZr$_{0.1}$Ce$_{0.7}$Y$_{0.2}$O$_{3-\delta}$ asymmetric cermet membrane. *International Journal of Energy Research, 43*, 4959-4966. doi: 10.1002/er.4583
31. Fan D., Gao Y., Liu F., Wei T., Ye Z., Ling Y., Chen B., Zhang Y., Ni M., Dong D. (2021): Autothermal reforming of methane over an integrated solid oxide fuel cell reactor for power and syngas co-generation. *Journal of Power Sources, 513*, 230536. doi: 10.1016/j.jpowsour.2021.230536
32. Kumar A., Bhosale R.R., Malik S.S., Abusrafa A.E., Saleh M.A.H., Ghosh U.K., Al-Marri M.J., Almomani F.A., Khader M.M., Abu-Reesh I.M. (2016): Thermodynamic investigation of hydrogen enrichment and carbon suppression using chemical additives in ethanol dry reforming. *International Journal of Hydrogen Energy, 41*, 15149-15157. doi: 10.1016/j.ijhydene.2016.06.157